World Journal of Advanced Research and Reviews
eISSN: 2581-9615 CODEN (USA): WJARAI
Cross Ref DOI: 10.30574/wjarr
Journal homepage: https://wjarr.com/

(RESEARCH ARTICLE)

Check for updates

Cyanide removal by graphene-type oxidized biochar: kinetic study and adsorption isotherms

Yannick Daniel Djè [1], Zoungranan Yacouba [2,*], Dobi-Brice Kouadio Kouassi [1], Lynda Ekou [1] and Tchirioua Ekou [1]

[1] *Department of Chemistry, University NANGUI ABROGOUA, Abidjan, Côte d'Ivoire.*
[2] *Department of Mathematics, Physics and Chemistry, University Peleforo GON COULIBALY, Korhogo, Côte d'Ivoire.*

World Journal of Advanced Research and Reviews, 2024, 22(01), 660–670

Publication history: Received on 02 March 2024; revised on 10 April 2024; accepted on 12 April 2024

Article DOI: https://doi.org/10.30574/wjarr.2024.22.1.1075

Abstract

The use of biomass to convert it into valuable chemicals has recently attracted the interest of researchers. In this study, graphene-type oxidized biochar was synthesized by calcination using oil palm (Elaeis guineensis) seed hulls of the hybrid variety dura x pisifera as the main carbon source. Graphene-like oxidized biochar (BOGp) was prepared from BGp by modification of the oxidation method described by Panicker and colleagues. The influences of mass variation, concentration and contact time were investigated, respectively. The study showed that for 0.1 g of BOGp used in 50 mL of a 1 mg/L cyanide solution, the elimination rate is 65%, for an equilibrium time of 60 minutes, and the elimination process is chemisorption, which follows the pseudo-second-order kinetic model. Absorption is described by the Freundlich isotherm, confirming multilayer adsorption. The BOGp characteristics were analyzed using modern analytical methods. Characteristic analysis of the BOGp results indicated that it is a low-moisture material with a high ash percentage, a density of 0.71 and a zero-charge point pH of 4. DRX analysis showed characteristic graphitic carbon peaks at $2\theta \approx 26.03°$ followed by peaks at $2\theta \approx 10°$ and $2\theta \approx 43°$ characteristic of oxidized graphitic carbon. Infrared analysis revealed OH and C=O functions confirming BOGp oxidation and C=C and CH_2 groups corresponding to the skeletal vibration of the graphene sheet.

Keywords: Adsorption; Cyanide; Oxidation; Oil palm shells; Graphene; Models

1. Introduction

Gold panning is the small-scale extraction of gold, commonly practiced informally and illegally in several countries [1]. While this activity can be a source of income for local communities, it also causes significant damage to the environment, particularly in terms of pollution. Water pollution is one of the most significant forms of pollution associated with gold panning [2]. Gold miners use cyanide to extract gold from sediments, resulting in significant contamination of watercourses. Cyanide is an extremely dangerous chemical compound which, when released into the environment, can easily spread into rivers and groundwater [3]. This contamination can affect both drinking water and aquatic ecosystems. It is therefore important to take steps to prevent the release of cyanide into the environment. Some cyanide removal methods have been proposed, based on chemical [4], physical [5], biological [6,7] and even adsorption [8] techniques. Adsorption has attracted more interest in cyanide removal from wastewater due to its simplicity and the absence of hazardous chemicals [9]. Adsorption involves attaching an adsorbate to the surface of an adsorbent. This technique is promising, as there are many materials that could be developed as adsorbents for cyanide removal. Recent studies have focused on materials, including activated carbon [10], zeolite [11], ion exchange resin [12] and graphene [8]. Graphene is a single layer of sp2-hybridized carbon of hydrophilic nature and high charge density, which can enhance adsorption capacity [13]. Graphene can be obtained from natural or synthetic graphite. Obtaining synthetic graphite requires high temperatures and high costs [14]. In addition, graphene nanosheets obtained by exfoliation are

* Corresponding author: Zoungranan Yacouba; Email: zoungranan@gmail.com

unstable in water and tend to self-aggregate, which limits their ability to adsorb pollutants [15]. For this reason, carbonaceous biomass is increasingly being used as a precursor material to obtain graphene. In this study, palm kernel shells are used to obtain graphene-like biochar, which is then oxidized. The oxidized graphene-like biochar (BOGp) was characterized and used in aqueous cyanide removal tests. The kinetic parameters and adsorption isotherms of the reaction will be determined.

2. Material and methods

2.1. Bioresource

Oil palm (Elaeis guineensis) seed hulls of the hybrid variety dura x pisifera were used as a source of carbonaceous biomass. They were collected as domestic waste in the town of Bonoua (5°16 "N, 3°31 "W), south-east of the capital Abidjan (Côte d'Ivoire). The collected grains were transported to the laboratory.

2.2. Oxidation of graphene-type biochar

The synthesis of graphene-like biochar (BGp) has been described in our previous work [8]. This material will then be oxidized to obtain oxidized graphene-like biochar (BOGp). The oxidation method used is that described by Panicker and colleagues [16], with a few modifications. In a 500 mL beaker, 180 mL H_2SO_4 and 60 mL HNO_3 (3:1) are mixed. The mixture is heated to 80°C on a hot plate for 5 minutes, then 58 g of BGp is added and the mixture stirred with a glass rod for 85 minutes. The beaker is then transferred to an ice bath for 5 minutes, after which 10 g of $KMnO_4$ is slowly added to the solution over 40 minutes. After adding this quantity of $KMnO_4$, the beaker is placed under magnetic stirring at 250 rpm for 1 hour. The mixture is then heated again to 90°C for 25 minutes, while 200 ml of distilled water is gradually added throughout the process. To reduce excess KMnO4, 6 ml of 6% hydrogen peroxide (H_2O_2) is added. At this stage, a bright yellow solution is formed, visible on filtration. After filtration, the solid residue obtained is washed with distilled water to neutral pH, then oven dried (Memmert BM300, Schwabach, Germany) at 105°C for 24 hours. The solid, dried residue is oxidized graphene-like biochar (BOGp).

2.3. Characterization

2.3.1. Moisture content

In a ceramic crucible of mass m_0, a quantity of BGp is introduced and the mass m_1 of the assembly is taken at room temperature. The assembly is oven-dried at 105°C for 24 h, then weighed after cooling to obtain mass m_2. The process is repeated three times under the same temperature and pressure conditions. Moisture content (H) is calculated using the following formula:

$$H\,(\%) = \frac{m_1 - m_0}{m_2 - m_0} \times 100 \quad (1)$$

2.3.2. Zero-point-charge pH

The pHpzc, or zero-point charge pH, indicates the pH at which the total electrical charge on the BOGp is zero, either due to a complete absence of charge, or due to exact compensation of positive and negative charges. This parameter is important because of the involvement of electrostatic forces in the adsorption process. At pH levels above pH_{PZC}, the BOGp surface will carry an overall negative charge. In a series of seven 250 ml beakers, each containing 50 ml of NaCl (0.1 M) solution, we add HCl (0.1 M) or NaOH (0.1 M) to adjust initial pH values (pH_i) between 2 and 13. pH values are measured using a pH meter (Hanna HI 9813-5, Bucharest, Romania). We then added 1 g of BGp to each beaker and kept it under agitation for 48 hours. After stirring and filtration, we determine the final pH values (pH_f) of the solutions. The graphical representation pH_f - pH_i = f (pH_i) intersects the x-axis at the point of zero charge, denoted pHpzc

2.3.3. BOGp density

An empty 100 mL test tube is weighed (M0), filled to the gauge line with BOGp and weighed again (M1). The density of BOGp is given by:

$$d = \frac{M_1 - M_0}{100} \quad (2)$$

2.3.4. X-ray diffraction (XRD)

The structural phases of BOGp were determined by X-ray diffraction using the GBC-EMMA diffractometer (Braeside, Victoria, Australia) equipped with CuKα radiation (λ = 0.154 nm). Samples were analyzed in the 2θ range from 0.15 ◦ to 91 with a step size of 0.02.

2.3.5. FTIR analysis

FTIR was used to identify functional groups in the material (Nicolet 6700 Thermo-scientific, Boston, USA) using potassium bromide (KBr) pellets in the 650 to 4050 cm- 1 wavenumber range.

2.3.6. Specific surface area

The specific surface area, average pore volume and pore diameter of BGp and BOGp were determined by the BET method, using a surface and porosity analyzer (Micromeritics TriStar II 3020, Georgia, USA).

2.4. Batch adsorption study

2.4.1. Procedure

For all tests, a stock of potassium cyanide stock solution at C_0 = 50 mg/L was carefully prepared. The various C_i concentrations were obtained by diluting the stock solution. For each experiment, a mass of m=0.1 g of BOGp was placed in a 250 mL beaker containing a V_i=50 mL solution of potassium cyanide at concentration C_i. The beaker was then covered with film (Parafilm, PM-996, USA) to prevent cyanide evaporation. The cyanide-BOGp mixture is stirred at 300 rpm for a set time using a Heidolph Vibramax 100 vibrating shaker (Germany). After stirring, the mixture is filtered to obtain a final volume V_f. Residual cyanide analysis is performed by the pyridine-pyrazalone method, using HACH cyanide powder reagents in sealed bags (100 tests). A 10 ml volume of the filtrate undergoes complexation steps using cyanide reagents 3, 4 and 5 (cyaniver 3, cyaniver 4 and cyaniver 5). First, one sachet of cyaniver 3 is added to 10 ml of filtrate collected in a test tube. The tube is covered with Prafilm and shaken vigorously by hand for 30 seconds. It is then left to stand for a further 30 seconds. Next, the contents of cyanide 4 are added and shaken for 10 seconds, and finally the contents of cyanide 5 are added to the mixture and shaken again. Leave the mixture to stand for 30 minutes, during which time a blue color appears, indicating cyanide complexation. The same procedure is used with distilled water as a control sample. Optical densities are measured at 612 nm using a UV-visible photospectrometer (WFJ-752, China). Initial (C_i) and final (C_f) concentrations are determined using the calibration curve generated with a solution of potassium cyanide in distilled water. The adsorption capacity (q) of BOGp is calculated using the following equation:

$$q = \frac{C_i V_i - C_f V_f V}{m} \quad (3)$$

The percentage of cyanide removal E (%) at any contact time is determined by the following equation:

$$E(\%) = \frac{C_0 - C_t}{C_0} \times 100 \quad (4)$$

Where C_0 and C_t are the initial cyanide concentrations and at a contact time t respectively (mg/L).

2.4.2. Influence of some physicochemical parameters

The kinetics of the adsorption reaction were studied by placing 0.1 g of BOGp in each of eight (8) beakers containing 50 ml of cyanide solutions at C_i = 1 mg/L. Eight (8) stirring times were set for each beaker, namely 5 min, 10 min, 15 min, 30 min, 45 min, 60 min, 90 min and 120 min.

The impact of initial cyanide solution concentration on uptake efficiency was evaluated using concentrations of 1 mg/L, 2 mg/L, 4 mg/L, 6 mg/L, 8 mg/L and 10 mg/L. The agitation time for these tests was set at 1 hour under 300 rpm agitation.

The effect of varying masses of BOGp in solution was also assessed by contacting masses of 0.1 g, 0.2 g, 0.3 g, 0.4 g and 0.5 g of BOGp with a 1 mg/L potassium cyanide solution under one hour's agitation at 300 rpm.

3. Results and discussion

3.1. BOGp characterization

BOGp has a center content of 11.25%, this high ash content could be explained by metal enrichment during the graphitization process activated with metal chlorides. In addition, the material has a low moisture content (7.62%<10%), indicating that it is likely to have a high availability of pores and adsorption sites. The density of the material is 0.71 g/cm^3. This high-density value is linked to the quantity of mineral substance contained in BOGp. BET analysis revealed a specific surface area of 340.3151 m^2/g, for an average pore volume (BJH) of 0.023870 cm^3/g and an average diameter of 1.8990 nm. The specific surface area value observed in this study agrees with the work of Zhihao Zhang et al [17], who place it in the range 140 m^2/g to 432 m^2/g for oxidized graphene-type materials. The results of the pHpzc determination are shown in the figure, with positive surface charges for pH values below zero charge points (pHpzc=4). For pH values above pHpzc, the surface charges are negative.

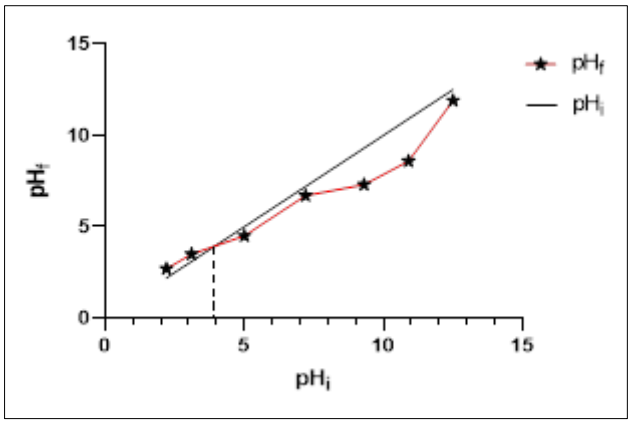

Figure 1 pH point of zero charge (pH$_{PZC}$)

The determination of the structural phases of BGp and BGpO by X-ray diffraction is shown in figure 2. The peak intensities of BGp and BOGp indicate a higher degree of graphitization, leading to a graphene-like structure [18]. This could be explained by the double oxidation of BGp. We also observe on the diffractogram of BGp and BOGp, the appearance of an intense peak (at 2θ ≈ 26.03°) characteristic of graphitic carbon [19] and peaks at 2θ ≈ 10° and 2θ ≈ 43° on the diffractogram of BGpO characteristic of oxidized graphitic carbon [19].

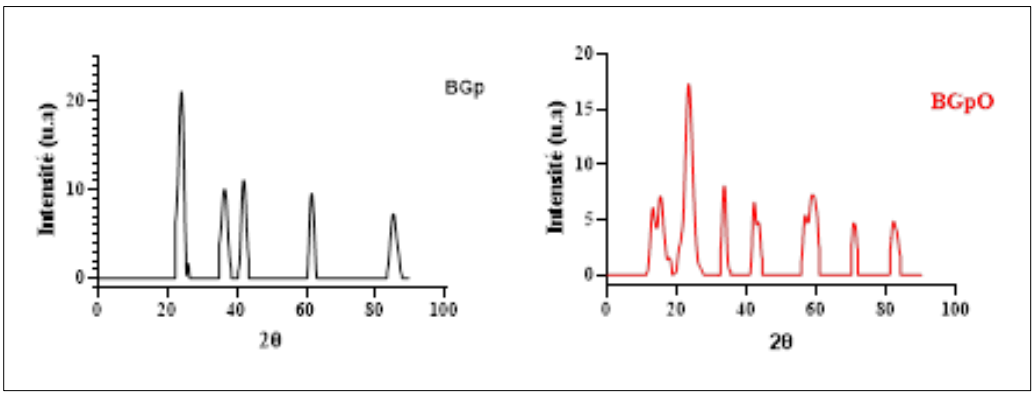

Figure 2 XRD of BGp and BOGp

The various functional groups in BOGp were studied using FTIR spectroscopy (FT-IR ALPHA II Spectrometer, Germany). The FT-IR spectra of BGp and BOGp are shown in Figure 3. The peaks between 3846.39 cm^{-1} and 3633.29 cm^{-1} correspond to the elongation vibrations of the OH group [20]. In the case of BGp, this is the group derived from the alcohol functions contained in the biomass. A multiplication of OH peaks is observed in the case of BOGp during the oxidation process, which can be explained by the simultaneous reduction of the C=O functions that appear in BGp at 1689.85cm^{-1} [21]. The appearance of a broad band characteristic of the carboxylic acid OH group. The C≡C function appearing at 2358.07 cm^{-1} in the BGp disappears at the BOGp, reflecting a probable oxidation reaction. The Alkyl nitrile

CN (R-CN) and Aryl nitrile CN (Ar-CN) functions appear respectively at 2361.44 cm^{-1} and 2160.88 cm^{-1} for the BGp however we observe a disappearance of the Alkyl nitrile function and a shift to 2173.9 cm^{-1} in the BOGp. At 1555 cm^{-1} and 1528 cm^{-1} nitrose groups are observed in BGp and BOGp respectively. The BOGp nitrose peak appears more intense, suggesting oxidation of the BGp hydroxylamines.

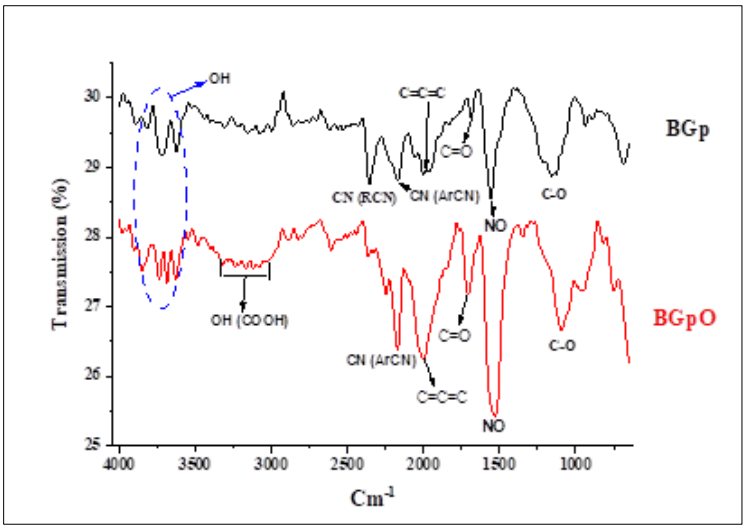

Figure 3 FTIR of BGp and BOGp

3.2. Effect of BOGp quantity

Figure 4 shows cyanide removal efficiency as a function of BOGp mass

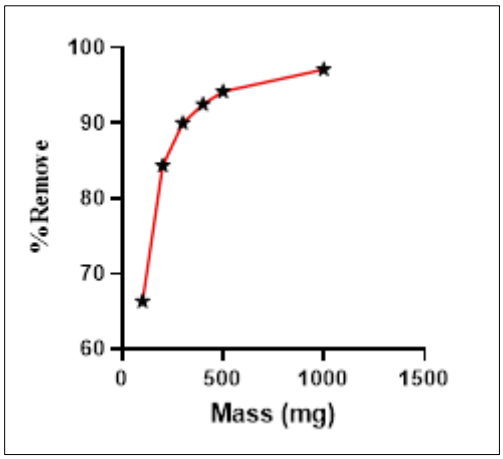

Figure 4 Percentage of cyanide removal as a function of BOGp quantity

The removal efficiency of BOGp increases from 66.32% to 97.01% when the mass of BOGp is increased from 0.1 g to 1 g. This increase is due to the increased volume of BOGp in solution, which provides more adsorption sites for cyanides. However, the formation of BOGp aggregates above 1 g may limit removal efficiency by reducing the number of adsorption sites available.

3.3. Adsorption kinetics and isotherm

3.3.1. Adsorption kinetics

The study of adsorption kinetics describes the rate at which cyanide is adsorbed by the adsorbent. Kinetic models are used to analyze the data and understand the adsorption mechanism. At an initial concentration of 1 mg/L, cyanide adsorption kinetics were studied by varying the contact time. Figure 5 shows that the rate of elimination increases rapidly during the first few contact times, then reaches a plateau after 60 minutes.

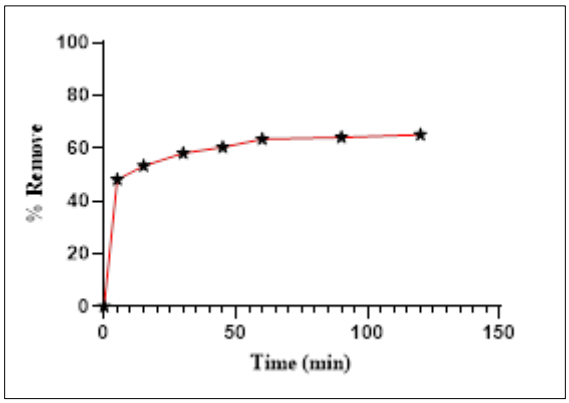

Figure 5 Cyanide removal rate as a function of BOGp contact time

Cyanide adsorption on BOGp is initially rapid, reaching a 65% removal rate within 60 minutes. This rapid initial adsorption is due to the availability of active sites on BOGp. As the active sites become saturated, adsorption slows down, reaching equilibrium in 60 minutes. Equilibrium is reached when the driving force, i.e. the difference in concentration between the solution and the BOGp, results in resistance to mass transfer [22].

Experimental results from the study of the effect of contact time were used to evaluate intraparticle, pseudo-first-order, pseudo-second order and Elovich diffusion models. The equations for each of these models are presented below.

Pseudo-first-order kinetics [23]:

$$\log(q_e - q_t) = \log(q_e) - \frac{k_1}{2.303}t \quad (5)$$

Pseudo-second-order kinetics [24]:

$$\frac{t}{q_t} = \frac{1}{k_2 q_e^2} + \frac{1}{q_e}t \quad (6)$$

Where q_e and qt represent the quantities of cyanide adsorbed at equilibrium and time t respectively; k_1 represents the pseudo-first-order kinetic constant; k_2 represents the pseudo-second-order kinetics; and t represents the adsorption time.

Elovich model [25]:

$$q = \frac{1}{\beta}\ln(\alpha\beta) + \frac{1}{\beta}\ln t \quad (7)$$

With α the initial adsorption rate (mg/g.min) and β the desorption constant related to surface area and reaction activation energy.

Intraparticle model:

$$q_t = k_d\sqrt{t} + C \quad (8)$$

kd (mg/g.min$^{0.5}$) is a diffusion constant and C is the boundary layer thickness [26].

Figure 6 shows the adsorption curves for cyanide on BOGp for the different models. Table 1 shows the model parameters.

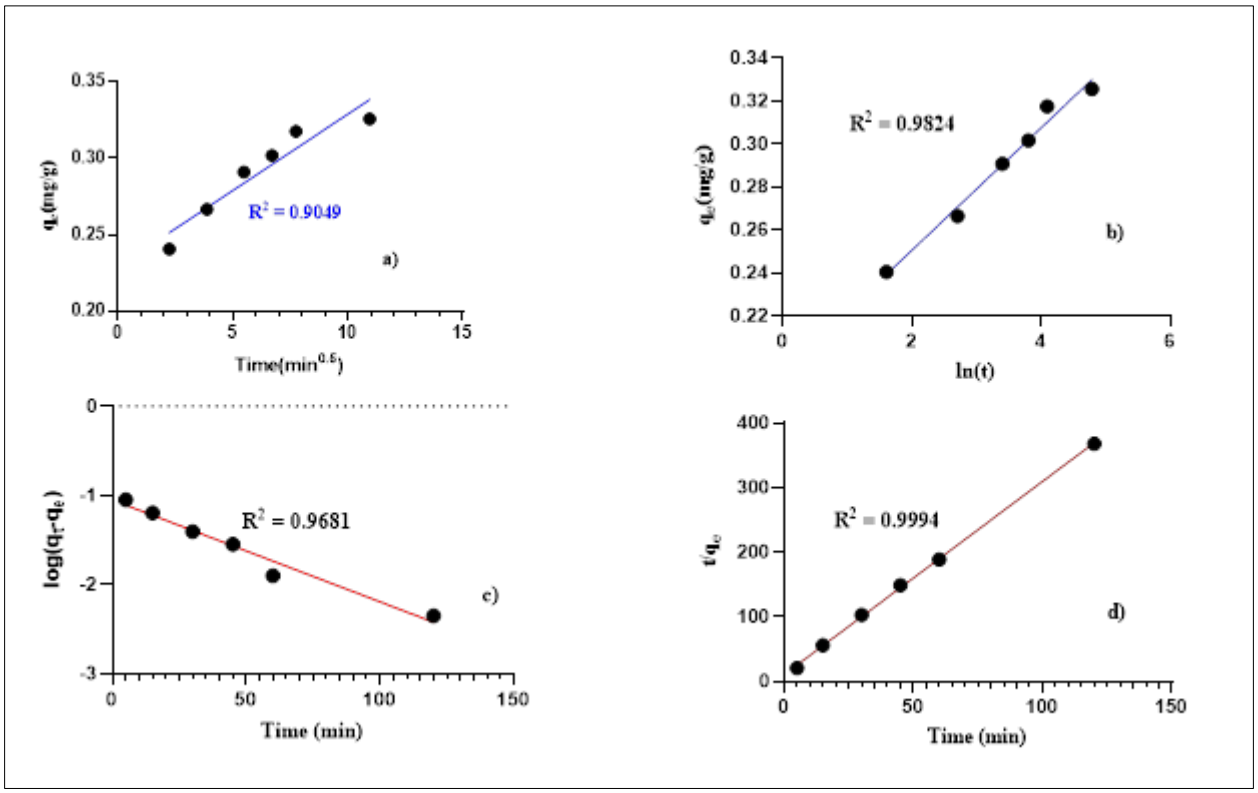

Figure 6 a) intraparticle, b) Elovich model, c) pseudo-first order, and d) pseudo-second order

Table 1 Parameters of adsorption kinetic models

	Pseudo-first order			**Pseudo-second order**			**Elovich**			**intraparticle**		
q_{exp}	k_1	q_e	R^2	k_2	q_e	R^2	α	β	R^2	k_d	C	R^2
0.33	0.02	0.088	0.97	0.85	0.33	0.99	25.41	35.09	0.98	0.01	0.23	0.90

Figure 6-a) shows the results of the study of intraparticle diffusion, enabling us to assess its impact on the overall reaction rate [27]. The linear regression of the adsorption curve does not pass through the origin, indicating that intraparticle diffusion is not the only factor limiting the reaction rate. Furthermore, the value of k_d = 0.01 mg/g.min0.5 suggests that intraparticle diffusion is an overall slow process [30]. The results of the Elovich model (Figure 6-b) show an excellent correlation with experimental results, suggesting that chemisorption plays a crucial role in cyanide adsorption on BOGp. This mechanism is also confirmed by the results of the pseudo-second-order model (figure 6-d), which predicts a quantity of adsorbed cyanide (q_{eth} = 0.33 mg/g) identical to the experimental value (q_{exp} = 0.33 mg/g). The cyanide adsorption process on BOGp does not follow the pseudo-first-order model (figure 6-c), ruling out the possibility of a significant contribution from Van der Waals forces to adsorption.

3.3.2. Adsorption isotherms

The study of adsorption isotherms makes it possible to evaluate the performance of adsorbents and determine important parameters such as adsorption capacity, saturation time and adsorption rate. In this study, adsorption isotherms were obtained by varying the initial cyanide concentration for a fixed contact time of 1 hour. Figure 7 shows the cyanide removal rate as a function of initial concentration.

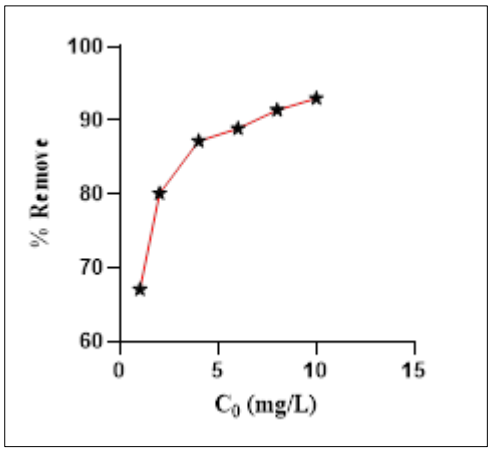

Figure 7 Cyanide removal rate as a function of initial concentration

The influence of initial cyanide concentration on adsorption was studied by varying the concentration from 1 to 10 mg/L. Figure 7 shows that the cyanide removal rate increases from 67% to 93% with increasing initial concentration. This increase is due to the increased driving force, which reduces the resistance to mass transfer between the aqueous (cyanide) and solid (BOGp) phases [22]. The results of the analysis were fitted to Langmuir, Freundlich and Temkin isothermal adsorption models.

The Langmuir equation, which describes the relationship between adsorbed quantity and equilibrium concentration, is given in the following linear form:[28]:

$$\frac{C_e}{q_e} = \frac{1}{q_m K_L} + \frac{1}{q_m} C_e \quad (9)$$

In the Langmuir equation, C_e (mg/L) represents the concentration of the cyanide solution, qe (mg g^{-1}) represents the amount of cyanide adsorbed at equilibrium, K_L is the Langmuir constant and q_m the maximum capacity of cyanide adsorbed. The Langmuir separation factor R_L, which assesses the affinity of the adsorbate for the adsorbent, is given by the following relationship:

$$R_L = \frac{1}{1 + K_L C_0} \quad (10)$$

When $R_L > 1$ adsorption is unfavorable, linear for $R_L = 1$, favorable when $0 < R_L < 1$ and irreversible if $R_L = 0$.

The Freundlich isotherm describes a nonlinear adsorption process on a heterogeneous surface in a multilayer approach. The Freundlich equation is given by the following relation [29].

$$\log(q_e) = \log K_F + \frac{1}{n} \log C_e \quad (11)$$

Where K_F (L/mg) is the adsorption capacity and $1/n$ (L/g) is the adsorption intensity; it also shows the relative energy distribution and heterogeneity of adsorbed sites.

The Temkin isotherm is an isothermal adsorption model that describes the adsorption of an adsorbate on a heterogeneous surface. It assumes of a decrease in adsorption energy followed by a decrease in adsorbate concentration [30, 31]. The linear form is:

$$q_e = \frac{RT}{b_T} \ln K_T + \left(\frac{RT}{b_T}\right) \ln C_e \quad (12)$$

Where K_T is the Temkin coefficient related to the nature of the adsorbent and adsorbate and b_T (J/mol) the coefficient related to the average adsorption energy.

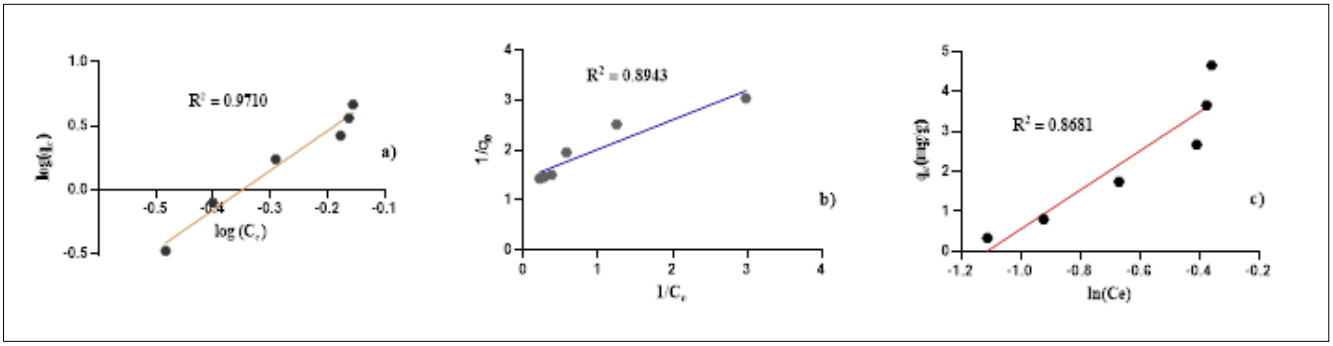

Figure 8 Adsorption isotherm models tested: a) Freundlich; b) Langmuir and c) Temkin.

Table 2 Parameters of various adsorption isotherms tested.

		Freundlich				**Langmuir**				**Tempkin**			
Parameters		R^2	1/n	K_F		R^2	q_{max}	R_L		R^2	K_T	b_T	
		0.97	1.08	12.16		0.89	0.70	0.10		0.87	1.74	1424.61	

The experimental results for cyanide adsorption on BOGp do not conform to the Langmuir model (fig.8-b). This suggests that the adsorption surface is not homogeneous and that there are significant interactions between the adsorbed cyanide layers. However, R_L = 0.1 indicates that cyanide adsorption is favorable. Temkin's model (Fig.8-b) correlates well with the experimental results. The high value of the bT constant, equal to 1424.60 J/mol, indicates that the cyanide adsorption reaction on BOGp is exothermic [32]. The Freundlich model also correlates well with experimental results, with a coefficient of determination R^2 of 0.97, and the value of the heterogeneity factor n is 1.08 > 1. This indicates that the Freundlich model effectively describes cyanide adsorption and follows an L-type isotherm [33]. This result also suggests multilayer chemisorption on a heterogeneous surface [34].

4. Conclusion

A methodology was used to transform palm kernel hulls into graphene-like oxidized biochar (BOGp) using a combination of graphitization-activation and double oxidation processes. X-ray diffraction (XRD) analysis revealed changes in the material's crystal structure. Fourier Transform Infrared Spectroscopy (FTIR) analysis detected the presence of functional groups such as alcohol and carboxyl functions, indicating oxidation of the material. BOGp has a low moisture content, medium density and zero surface charge (pHpzc = 4). BOGp has been successfully used to remove cyanide from a synthetic aqueous solution. Adsorption tests demonstrated that cyanide adsorption on BOGp is favorable and follows a pseudo-second-order kinetic model, indicating chemisorption. This conclusion is corroborated by the study of adsorption isotherms, which show L-type adsorption, in accordance with the Freundlich model. In addition, a correlation with the Tempkin model was observed, confirming chemisorption, and revealing that the cyanide adsorption reaction on BOGp is exothermic. This study highlights the possibility of converting readily available biomass waste into a material like oxidized graphene for the removal of pollutants such as cyanide used in gold panning.

Compliance with ethical standards

Disclosure of conflict of interest

No conflict of interest to be disclosed.

References

[1] Ngom NM, Mbaye M, Baratoux D, Baratoux L, Ahoussi KE, Kouame JK, et al. Recent expansion of artisanal gold mining along the Bandama River (Côte d'Ivoire). International Journal of Applied Earth Observation and Geoinformation 2022;112:102873. https://doi.org/10.1016/j.jag.2022.102873.

[2] Obeng EA, Oduro KA, Obiri BD, Abukari H, Guuroh RT, Djagbletey GD, et al. Impact of illegal mining activities on forest ecosystem services: local communities' attitudes and willingness to participate in restoration activities in Ghana. Heliyon 2019;5:e02617. https://doi.org/10.1016/j.heliyon.2019.e02617.

[3] Fashola M, Ngole-Jeme V, Babalola O. Heavy Metal Pollution from Gold Mines: Environmental Effects and Bacterial Strategies for Resistance. International Journal of Environmental Research and Public Health 2016;13:1047. https://doi.org/10.3390/ijerph13111047.

[4] Zhao C, Yuan Y, Qu G, Li J, Liu G, Yuan Z, et al. Simultaneously remove Phosphine, hydrogen sulfide and hydrogen Cyanide: Synergistic effect of micro-electrolysis and liquid-phase catalytic electrolysis. Separation and Purification Technology 2023:125085. https://doi.org/10.1016/j.seppur.2023.125085.

[5] Botz MM, Mudder TI, Akcil AU. Cyanide Treatment. Gold Ore Processing, Elsevier; 2016, p. 619–45. https://doi.org/10.1016/B978-0-444-63658-4.00035-9.

[6] Razanamahandry LC, Andrianisa HA, Karoui H, Kouakou KM, Yacouba H. Biodegradation of free cyanide by bacterial species isolated from cyanide-contaminated artisanal gold mining catchment area in Burkina Faso. Chemosphere 2016;157:71–8. https://doi.org/10.1016/j.chemosphere.2016.05.020.

[7] Alvillo-Rivera AJ, Garrido-Hoyos SE, Rosano-Ortega G. Optimization of Factors for the Biological Treatment of Free and Complexed Cyanide. Processes 2023;11:2063. https://doi.org/10.3390/pr11072063.

[8] Yannick DD, Zoungranan Y, Dobi-Brice KK, Lynda E, Tchirioua E, Djè Daniel Yannick, Yacouba Zoungranan, Kouassi Kouadio Dobi-Brice EL, et al. Graphene-Like Biochar from Agricultural Waste for Cyanide Removal: Kinetic Study and Adsorption Isotherms. Science Journal of Chemistry 2023;11:189–96. https://doi.org/10.11648/j.sjc.20231105.12.

[9] Pérez-Cid B, Calvar S, Moldes AB, Manuel Cruz J. Effective Removal of Cyanide and Heavy Metals from an Industrial Electroplating Stream Using Calcium Alginate Hydrogels. Molecules 2020;25:5183. https://doi.org/10.3390/molecules25215183.

[10] Wang X, Wang X, Tan H, Hu Z, Deng S, Li Y. Removal of Hydrogen Cyanide by Using Activated Carbon: The Effect of Adsorption Condition and Chemical Modification. Journal of Biobased Materials and Bioenergy 2015;9:545–52. https://doi.org/10.1166/jbmb.2015.1554.

[11] Noroozi R, Al-Musawi TJ, Kazemian H, Kalhori EM, Zarrabi M. Removal of cyanide using surface-modified Linde Type-A zeolite nanoparticles as an efficient and eco-friendly material. Journal of Water Process Engineering 2018;21:44–51. https://doi.org/10.1016/j.jwpe.2017.11.011.

[12] Simsek H, Kobya M, Khan E, Bezbaruah AN. Removal of aqueous cyanide with strongly basic ion-exchange resin. Environmental Technology 2015;36:1612–22. https://doi.org/10.1080/09593330.2014.999829.

[13] Banerjee P, Sau S, Das P, Mukhopadhayay A. Optimization and modelling of synthetic azo dye wastewater treatment using Graphene oxide nanoplatelets: Characterization toxicity evaluation and optimization using Artificial Neural Network. Ecotoxicology and Environmental Safety 2015;119:47–57. https://doi.org/10.1016/j.ecoenv.2015.04.022.

[14] Sierra U, Álvarez P, Blanco C, Granda M, Santamaría R, Menéndez R. Cokes of different origin as precursors of graphene oxide. Fuel 2016;166:400–3. https://doi.org/10.1016/j.fuel.2015.10.112.

[15] Xiao X, Chen B, Zhu L, Schnoor JL. Sugar Cane-Converted Graphene-like Material for the Superhigh Adsorption of Organic Pollutants from Water via Coassembly Mechanisms. Environmental Science and Technology 2017;51:12644–52. https://doi.org/10.1021/acs.est.7b03639.

[16] Panicker NJ, Das J, Sahu PP. Synthesis of highly oxidized graphene (HOG) by using HNO3 and KMnO4 as oxidizing agents. Materials Today: Proceedings 2021;46:6270–4. https://doi.org/10.1016/j.matpr.2020.05.037.

[17] Zhang Z, Schniepp HC, Adamson DH. Characterization of graphene oxide: Variations in reported approaches. Carbon 2019;154:510–21. https://doi.org/10.1016/j.carbon.2019.07.103.

[18] Chang B, Guo Y, Li Y, Yin H, Zhang S, Yang B, et al. Graphitized hierarchical porous carbon nanospheres: simultaneous activation/graphitization and superior supercapacitance performance. Journal of Materials Chemistry A 2015;3:9565–77. https://doi.org/10.1039/C5TA00867K.

[19] Trikkaliotis DG, Christoforidis AK, Mitropoulos AC, Kyzas GZ. Graphene Oxide Synthesis, Properties and Characterization Techniques: A Comprehensive Review. ChemEngineering 2021;5:64. https://doi.org/10.3390/chemengineering5030064.

[20] Alam SN, Sharma N, Kumar L. Synthesis of Graphene Oxide (GO) by Modified Hummers Method and Its Thermal Reduction to Obtain Reduced Graphene Oxide (rGO)*. Graphene 2017;06:1–18. https://doi.org/10.4236/graphene.2017.61001.

[21] Krishnamoorthy K, Veerapandian M, Yun K, Kim S-J. The chemical and structural analysis of graphene oxide with different degrees of oxidation. Carbon 2013;53:38–49. https://doi.org/10.1016/j.carbon.2012.10.013.

[22] Dwivedi N, Balomajumder C, Mondal P. Comparative investigation on the removal of cyanide from aqueous solution using two different bioadsorbents. Water Resources and Industry 2016;15:28–40. https://doi.org/10.1016/j.wri.2016.06.002.

[23] LAGERGREN S. Zur theorie der sogenannten adsorption gelöster stoffe. Kungliga Svenska Vetenskapsakademiens 1898;24 (4):1–39.

[24] Ho, Y.S., Mc Kay G. Pseudo second order model for sorption processes. Process Biochemistry 1999;34 (5):451-459.

[25] Low MJD. Kinetics of Chemisorption of Gases on Solids. Chemical Reviews 1960;60:267–312. https://doi.org/10.1021/cr60205a003.

[26] Sahoo TR, Prelot B. Adsorption processes for the removal of contaminants from wastewater. Nanomaterials for the Detection and Removal of Wastewater Pollutants, Elsevier; 2020, p. 161–222. https://doi.org/10.1016/B978-0-12-818489-9.00007-4.

[27] Singh N, Balomajumder C. Simultaneous removal of phenol and cyanide from aqueous solution by adsorption onto surface modified activated carbon prepared from coconut shell. Journal of Water Process Engineering 2016;9:233–45. https://doi.org/10.1016/j.jwpe.2016.01.008.

[28] Günay A, Arslankaya E, Tosun Iİ. Lead removal from aqueous solution by natural and pretreated clinoptilolite: Adsorption equilibrium and kinetics. Journal of Hazardous Materials 2007;146:362–71. https://doi.org/10.1016/j.jhazmat.2006.12.034.

[29] DeMessie JA, Sorial GA, Sahle-Demessie E. Removing chromium (VI) from contaminated water using a nano-chitosan–coated diatomaceous earth, 2022, p. 163–76. https://doi.org/10.1016/B978-0-323-90763-7.00005-6.

[30] Aharoni C, Ungarish M. Kinetics of activated chemisorption. Part 2.—Theoretical models. Journal of the Chemical Society, Faraday Transactions 1: Physical Chemistry in Condensed Phases 1977;73:456. https://doi.org/10.1039/f19777300456.

[31] Vadi M, Mansoorabad AO, Mohammadi M, Rostami N. Investigation of Langmuir, Freundlich and Temkin Adsorption Isotherm of Tramadol by Multi-Wall Carbon Nanotube. Asian Journal of Chemistry 2013;25:5467–9. https://doi.org/10.14233/ajchem.2013.14786.

[32] Edet UA, Ifelebuegu AO. Kinetics, Isotherms, and Thermodynamic Modeling of the Adsorption of Phosphates from Model Wastewater Using Recycled Brick Waste. Processes 2020;8:665. https://doi.org/10.3390/pr8060665.

[33] Bonilla-Petriciolet A, Mendoza-Castillo DI, Dotto GL, Duran-Valle CJ. Adsorption in Water Treatment. Reference Module in Chemistry, Molecular Sciences and Chemical Engineering, Elsevier; 2019, p. 1. https://doi.org/10.1016/B978-0-12-409547-2.14390-2.

[34] Mekhalef Benhafsa F, Kacha S, Leboukh A, Belaid KD. Étude comparative de l'adsorption du colorant Victoria Bleu Basique à partir de solutions aqueuses sur du carton usagé et de la sciure de bois. Revue Des Sciences de l'eau 2018;31:109–26. https://doi.org/10.7202/1051695ar